Bull. Soc. géol. Fr., 2003, t. 174, n° 6, pp. 529-543

Volume spécial :
Géodynamique de l'Asie du Sud-Est

Dynamics and age of formation of the Seram-Ambon ophiolites (Central Indonesia)

CHRISTOPHE MONNIER[1], JACQUES GIRARDEAU[1], HARIADY PERMANA[1-2], JEAN-PIERRE REHAULT[3], HERVÉ BELLON[3] et JO COTTEN[3]

Key words. – Southeast Asia, Ophiolite, High-Mg arc-tholeiites, Back-arc basin basalts, Transtensive rifting

Abstract. – The Seram-Ambon ophiolitic series comprise peridotites, websterites, gabbros and lavas. Petro-geochemical data show that the peridotites are weakly depleted rocks, except for the rare Cpx-free harzburgites. They underwent a sub-solidus metamorphic re-equilibration in the plagioclase field. The associated websterites and gabbros display various chemical features, allowing to define 3 types of websterites and 2 groups of gabbros. They have mostly BAB characteristics (presence of negative anomalies in Nb, Zr, Ti and Y), except the group 2 gabbros which have N-MORB features and the type 3 websterites which bear adakitic affinities. Lavas also display a variety of compositions, including high-Mg IAT and Mg-rich BABB with sub-alkaline affinities. Both IAT and BABB display high Th/Nb ratios which support an origin close to a continental crust environment.

Our 20 to 15 Ma $^{40}K/^{40}Ar$ ages calculated for the BABB and 15-9 Ma for the IAT show that the basin and arc formed in a very short span of time, before their obduction 9-7 Ma ago [Linthout *et al.*, 1997]. Considering the paleogeographic situation in the Miocene [Haile, 1979 ; Haile, 1981] and our data, we propose that the Seram-Ambon ophiolites formed during the early Miocene in a small, short-lived (10 Ma), transtensive basin bordered on its east by an active margin and on its western part by a passive continental margin over which it was later obducted towards the SW direction.

Dynamique et âge de formation des ophiolites de Seram-Ambon (Indonésie centrale)

Mots-clés. – Asie du Sud-Est, ophiolite, tholéiites riches en MgO, basaltes arrière-arc, rifting transtensif.

Résumé. – L'île de Seram-Ambon est située au nord de la mer de Banda entre les îles de Sulawesi et de Nouvelle Guinée (fig. 1A). Sa position actuelle montre que son évolution géotectonique est et a été fortement liée, depuis le milieu du Cénozoïque, aux mouvements respectifs de la plaque Australienne qui remonte vers le NNW à raison de 7 cm.an^{-1} et de la plaque Philippine qui se déplace vers l'ouest à une vitesse d'environ 10 cm.an^{-1} [Minster et Jordan, 1978 ; De Mets *et al.*, 1990].

Plusieurs fragments d'ophiolites y sont présents. Ils sont pour l'essentiel localisés dans la partie ouest de l'île de Seram (fig. 1B), sur les petites îles de Kelang situées à l'ouest et sur l'île d'Ambon présente au sud-est [Tjokrosapoetro et Budhitrisna, 1982] (fig. 1C). Ces trois secteurs réunis présentent tous les termes classiques d'une séquence ophiolitique, avec des péridotites, pyroxénites, gabbros et basaltes, mais aucun d'entre eux ne présente la totalité des termes d'une série ophiolitique complète. Les péridotites sont essentiellement des lherzolites à plagioclase, des harzburgites à spinelle riches en Cpx (3-3,5 %) pouvant contenir jusqu'à 2,2 % de plagioclase, et plus rarement des harzburgites sans Cpx qui contiennent quelques rubannements d'orthopyroxénites. Ces péridotites sont localement recoupées par des filonnets de chromitites, par des filons ou poches de webstérites de compositions chimiques variées (types 1, 2 et 3), généralement à cœur gabbroïque (groupes 1 et 2) et par des filons basaltiques.

L'origine et la mise en place de ces séries ophiolitiques restent encore très controversées [Katili, 1975 ; Hutchison, 1977 ; Milson, 1977 ; Hamilton, 1979]. D'après Linthout *et al.* [1997], elles représenteraient un ancien fragment océanique d'âge miocène qui se serait formé à la suite d'une ouverture en milieu continental le long de la marge ouest australienne, leur obduction sur Seram datant de 9-7 Ma.

Les données pétrologiques et géochimiques que nous présentons dans ce travail montrent que les péridotites ont un caractère faiblement résiduel bien qu'étant très riches en olivine (tabl. I). Les faibles teneurs en C# du spinelle (C# = Cr/[Cr+Al]) des harzburgites sans Cpx (C# = 0,40 en moyenne) contrastent avec celles plus élevées des harzburgites riches en Cpx (0,43<Cr#<0,53) et des lherzolites à plagioclase (0,47<Cr#<0,56 – fig. 3B). Les spinelles se caractérisent par de fortes teneurs en titane (Ti>50 millications – fig. 3C), de même que les pyroxènes (Ti_{Opx}>7 millications, Ti_{Cpx}>14 millications) des lherzolites à plagioclase. Ces fortes teneurs en Ti seraient associées à la formation métamorphique du plagioclase lors de la rééquilibration sub-solidus de ces roches dans le faciès à plagioclase (fig. 3D) lors de leur remontée [Kornprobst et Tabit, 1988 ; Li, 1991 ; Cornen *et al.*, 1996 ; Charpentier, 2000]. Les lherzolites à plagioclase présentent des spectres de terres-rares homogènes (environ 2 fois les valeurs chondritiques) dont l'appauvrissement en terres-rares légères (0,1<La/Sm<0.3 – fig. 4A) traduit un taux de fusion partielle modéré. Les harzburgites riches en Cpx montrent de plus faibles concentrations en terres-rares lourdes et en intermédiaires (environ 0,5 fois les

[1]Laboratoire de Planétologie et Géodynamique, UMR-CNRS 6112, Université de Nantes, 44322 Nantes cedex 3, France.
[2]Earth Dynamic and Geological Hazard Division, Research Center for Geotechnology, LIPI Complex, JI. Sangkuriang Bandung, 40135, Indonesia.
[3]Domaines Océaniques, UMR 6538, UBO-IUEM, 29280 Plouzané, France.
Manuscrit déposé le 24 avril 2002 ; accepté après révision le 26 juin 2003.

valeurs chondritiques – fig. 4B) caractéristiques de taux de fusion plus importants. Les très faibles concentrations en terres-rares des harzburgites sans Cpx (0,1-0, 3 fois les chondrites – fig. 4C, valeurs inhabituelles si on compare ces valeurs avec celles des péridotites océaniques [Niu, 1997 ; Niu et Hékinian, 1997]), sont par contre les témoins d'un manteau fortement résiduel. Si les enrichissements en terres-rares légères peuvent être interprétés comme résultant d'un effet chromatographique (e.g. Takazawa *et al.*[1992 ; 2000]), il ne peut être exclu qu'un processus métasomatique subséquent à la fusion partielle de ces roches soit à leur origine, ainsi que cela a été suggéré par Weichert *et al.* [1996].

Certains cumulats mantelliques (webstérites de type 1 et gabbros du groupe 1) sont caractérisés par des spectres de terres-rares plats (6-10 fois les valeurs chondritiques), légèrement appauvris en terres-rares légères (fig. 5A-B, tabl. II). Les formes spectrales laissent supposer que ces cumulats ont évolué par cristallisation fractionnée en accord avec les observations de terrain qui montrent que ces roches sont souvent associées. Les webstérites de type 2 et les gabbros du groupe 2 se distinguent des roches précédentes par leurs très forts appauvrissements en terres-rares légères ($0{,}02<(La/Yb)_N<0{,}04$ – fig. 5A-B), traduisant une cristallisation à partir de liquides magmatiques provenant de taux de fusion plus importants. Par opposition, les webstérites de type 3 se caractérisent par de très forts enrichissements en terres-rares légères ($3{,}40<(La/Yb)_N<24{,}00$ – fig. 5C) et par de faibles à très faibles concentrations en terres-rares lourdes ($0{,}1<Yb<1{,}0$ ppm). En accord avec les valeurs élevées en Na mesurées dans les Cpx (fig. 3E), ceci suggère une origine des sources plus profonde et riche en grenats.

La plupart de ces cumulats ont cependant la particularité de présenter des spectres multi-éléments ayant des caractéristiques géochimiques similaires à celles des laves associées (anomalies négatives en Nb, Zr, Ti, Y, voir paragraphes suivants), ce qui montre que leur mise en place dans le manteau pourrait être liée à une remontée du manteau générée par l'ouverture du bassin arrière-arc.

Les roches effusives présentent de faibles variations des concentrations en SiO_2 (46,60-58,30 % – tabl. III). Elles sont également caractérisées par des teneurs élevées en Al_2O_3 (16,60 % en moyenne) et par de faibles concentrations en TiO_2 et K_2O (0,75 et 0,15 % en moyenne réciproquement).

Les laves dont les concentrations en Na_2O sont les plus élevées ($1{,}47\ \%<Na_2O<2{,}79\ \%$ – fig. 3F) présentent des spectres de terres-rares typiques de basaltes de rides océaniques (MORB) (fig. 6B). Elles se caractérisent néanmoins par des enrichissements en éléments fortement incompatibles (par exemple : U, Th) qui, associés à la présence de fortes anomalies négatives en Nb ($3{,}0<(La/Nb)_N<5{,}0$) et dans une moindre mesure en Zr, en Ti et en Y, suggèrent une formation dans un bassin arrière-arc [Saunders et Tarney, 1984 ; Monnier *et al.*, 1995]. Le caractère très primitif de certaines d'entre elles ($MgO>10\ \%$) traduirait une mise en place précoce dans un bassin qui pourrait s'être par ailleurs ouvert en bordure d'une marge continentale compte-tenu des fortes concentrations en Th mesurées ($Th/Nb=0{,}62$) [Auzende *et al.*, 1990 ; Eissen *et al.*, 1998].

Les autres laves associées ont des teneurs plus faibles en Na_2O ($Na_2O<1{,}15\ \%$). Elles sont caractérisées par de forts enrichissements en terres-rares légères (20 à 100 fois les valeurs chondritiques) et présentent des anomalies négatives en Nb et en Ta (fig. 6A), typiques des tholéiites d'arc faiblement potassiques ($0{,}06\ \%<K_2O<0{,}79\ \%$). Les fortes concentrations en MgO (>10 %) de certaines d'entre elles, comparables à celles rencontrées dans les basaltes arrière-arc, suggèrent qu'elles sont issues de liquides primaires pouvant s'être formés lors des premiers stades de l'édification d'un arc volcanique (e.g. Jonhson *et al.* [1980 ; 1990]).

Les études pétro-géochimiques des unités ophiolitiques de Seram-Ambon ont permis de montrer que les péridotites représentent un manteau partiellement fondu, ayant subi un rééquilibrage dans le faciès à plagioclase, probablement lors de sa décompression dans un contexte d'ouverture en bordure de marge continentale. Ces études ont également permis de mettre en évidence l'existence de tholéiites d'arc dont certaines sont caractérisées par de fortes teneurs en MgO, ce qui pourrait suggérer une origine lors des premiers stades de l'édification d'un arc volcanique et de BABB (associées dans l'espace aux tholéiites d'arc) dont certaines sont elles-mêmes riches en MgO. Les fortes affinités géochimiques existant entre les tholéiites d'arc et les basaltes arrière-arc plaideraient pour une ouverture du bassin océanique dans les premiers stades du processus de subduction. La remontée du manteau arrière-arc se serait accompagnée de la mise en place de nombreux cumulats mantelliques (webstérites et gabbros) ayant aussi des caractéristiques arrière-arc, à l'exception des gabbros du groupe 2 qui ont des signatures de N-MORB et d'un échantillon de webstérite de type 3 à affinité adakitique.

Les âges radiochronologiques ($^{40}K/^{40}Ar$ – tabl. IV) obtenus sur les basaltes arrière-arc (20-15 Ma) montrent bien que le bassin marginal s'est ouvert au cours des premiers stades de l'édification d'un arc volcanique dont seulement des jeunes témoins ont pu être datés (15-9 Ma). Ce dernier âge (9 Ma) est contemporain de celui de l'exhumation de l'ophiolite sur l'île de Seram qui aurait débuté vers 9,5 Ma pour s'achever vers 7 Ma [Linthout *et al.*, 1996, 1997]. Ceci indique un contexte géotectonique particulièrement rapide pour la formation et l'exhumation de l'ophiolite. Compte tenu de la position paléo-géographique de l'île de Seram qui aurait été bordée à l'est par un domaine océanique lors de sa remontée vers le nord au Miocène [Haile, 1979 ; Haile, 1981] et de nos données géochimiques, nous proposons que ce bassin s'est formé dans un système transtensif, à durée de vie limitée (10 Ma), bordé à l'ouest par la marge continentale de Seram (fig. 7). L'obduction de l'ophiolite au Miocène supérieur se serait effectuée du NE vers le SW, si on prend en compte la rotation de 70° qu'a subi l'île lors de sa migration vers le nord [Linthout *et al.*, 1997], ce qui résulte de nos observations structurales qui indiquent, pour la position actuelle de Seram, des cisaillements du NW vers le SE (fig. 2) [Permana, 1998].

INTRODUCTION

The Seram island is located in the North of the Banda sea between the Sulawesi and New Guinea islands (fig. 1A). With a surface close to 18 000 km^2, this island is bordered in its southwestern part by the Ambon islands (fig. 1B) and in its western part by the Manipa, Kelang and Bonao islands (fig. 1C). All these islands are located at the boundary of two large major plates (fig. 1A) : the Australian plate which moves up towards the NNW at a rate of 7 $cm.y^{-1}$ and the Philippine one which moves towards the west at 10 $cm.y^{-1}$[Minster and Jordan, 1978 ; De Mets *et al.*, 1990]. The current position of the Seram island shows that its geotectonic evolution has been strongly related to the respective movements of these two plates, particularly during the Cenozoic when the Australian plate collided with the Eurasian continent [De Smet *et al.*, 1989]. However, during Cenozoic times, the tectonic evolution of Seram remains poorly known. It is currently proposed that Seram represents, as well as Buru and Timor islands, a Paleozoic-Triassic continental shelf fragment initially linked to the Australian margin, and probably located along the paleo-subduction zone of the Banda arc [Katili, 1975 ; Hamilton, 1979]. Paleomagnetic studies indicate that, since the late Triassic, the Seram-Buru microplate has moved 11° northward and rotated 92° anticlockwise, of which 2° and 74°, respectively, took place since the late Miocene [Haile, 1981]. This rotation, initially controlled by the Australian and Pacific plates convergences, would have been carried out along a transform fault in the western boundary of the Banda paleo-sea [Daly *et al.*, 1987 ; De Smet *et al.*, 1989 ; Daly *et al.*, 1991]. During the middle to late Miocene, numerous small Plio-Pleistocene basins formed in relation to the Pacific plate subduction under the Seram-Buru microblock [Audley-Charles *et al.*, 1979 ; De Smet *et al.*, 1989]. Finally, during the Pleistocene, the pristine collision between the Australian and Eurasian continental plates produced the upwelling relief, that reaches now up to 3000m above the sea level [De Smet *et al.*, 1989].

Several fragments of ophiolitic series are present on Seram, Kelang and Ambon islands (fig. 1). In Seram, they are mainly located in its western part (Kaibobo, fig. 1B), while ultramafic rocks have been described in its central and eastern parts [Tjokrosapoetro and Budhitrisna, 1982]. To this day, the origin and the space-time obduction of this ophiolite remain still under discussion. But many authors [Katili, 1975 ; Hutchison, 1977 ; Milson, 1977 ; Hamilton, 1979] have proposed that the ophiolite could have originated in the Banda Sea, because of the presence of abundant peridotite outcrops on the Ambon island, located southward (fig. 1B). Recently, based on a P-T path model inferred from the study of plagioclase bearing peridotites, Linthout *et al.* [1997] have concluded that this ophiolite formed by rifting of a continental shelf during the early Miocene to middle Miocene, in between the Australian plate and the Buru-Seram microblock. Its obduction onto Seram would have occurred between 9.5 Ma and 7 Ma [Linthout *et al.*, 1997].

In this paper, we present new petrological, geochemical (major and trace elements) and radiochronological datations ($^{40}K/^{40}Ar$) on the main lithologies (peridotites, websterites, gabbros and basalts) of the ophiolite series from Seram and Ambon islands, in order to constrain magmatic processes at the origin of their formation and reconstruct their paleo-evolution.

THE OPHIOLITIC UNITS

Remnants of ophiolitic series are present in the western part of the Seram island, and to a lesser extent, on the Ambon and Kelang islands (fig. 1). They contain all terms of an ophiolitic sequence, from the peridotites and gabbros to the basalts. Unfortunately, the ophiolite is completely dismembered so that we have not been able to find any preserved magmatic contacts between the different units. The best outcrops are located in the north of Kaibobo and Talaga (Seram island – fig. 1B) and near Kilang and Seri (Ambon island – fig. 1C). Most of the samples recovered were picked out in streams along steep reliefs or cliffs accessible by boat from the sea (Serikambela and Kaibobo areas – fig. 1B).

At Seram, the ophiolite series comprise a 500 m-thick ultramafic unit that outcrops in the Kaibobo area (fig. 1B). It is mainly composed of fresh coarse-grained to porphyroclastic plagioclase-bearing lherzolites (pl-lherzolites) and of more altered spinel Cpx-rich harzburgites and Cpx-free harzburgites, containing locally cm-thick bands of orthopyroxenites parallel to the main foliation. Locally, the peridotites are crosscut by chromitic veins, millimetre-thick, and by thicker gabbros and websterites bands and dykes. Similar peridotites are also present in the Samauru, Ariate, Serikanbela and Ulatu areas (fig. 1B). In these sectors, websterites, gabbros and lavas are also present in large amounts and can be collected easily along streams.

In Ambon, rests of the ophiolite series crop out in Kilang and Seri areas and, in minor proportion, near Alang (fig. 1C). The rocks are strongly altered and correspond mainly to pl-lherzolites (more rarely spinel Cpx-rich harzburgites) that contain decimetre-thick bands of websterites with gabbros cores and more rarely of diabases. The peridotites are strongly foliated and locally transformed in talc and antigorite in the vicinity of recent granitic intrusions [Linthout and Helmers, 1994].

Overall, Pl-lherzolites and Cpx-rich harzburgites are much more abundant on the Seram and Ambon islands than the Cpx-free harzburgites which have been sampled only in restricted areas near Kaibobo and Talaga (Seram).

The metamorphic basement is represented by Paleozoic and Mesozoic micaschists [Audley-Charles *et al.*, 1979 ; Linthout *et al.*, 1989] in which fine-grained amphibolite and gneissic levels (biotite and garnet paragenesis) dated at 8 Ma [Linthout *et al.*, 1996] are locally intercalated. These rocks are sandwiched between peridotite slices (fig. 2B), the contact between these two series being marked by acid to basic granulites [Permana, 1998]. They present a well-marked foliation that is gently folded, mostly dips toward the north and bears a well-oriented N150° stretching lineation (fig. 2A). The sense of shear, determined from C/S bands, indicates thrusting towards the SE of the ophiolitic pile onto the continental basement [Permana, 1998].

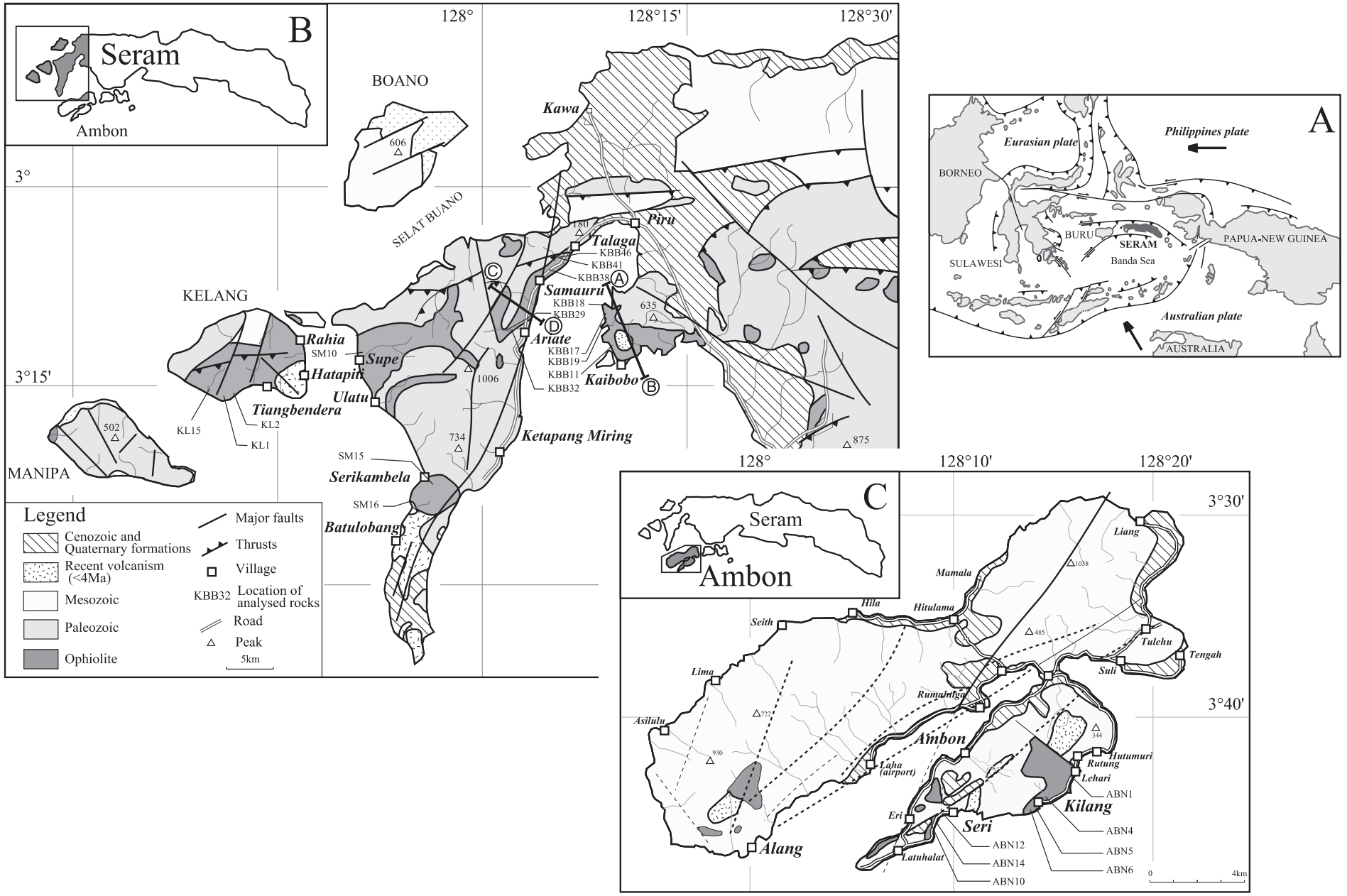

FIG. 1. – A) Location of Seram-Ambon islands in the central part of the indonesian archipelago. Simplified geological and tectonic maps of B) the western part of Seram and C) Ambon islands showing the main ophiolitic series (modified from Tjokrosapoetro and Budhitrisna [1982]).

FIG. 1. – A) *Situation générale de Seram-Ambon dans la partie centrale de l'archipel indonésien. Cartes géologiques et tectoniques simplifiées* B) *de la partie ouest des îles de Seram et* C) *de Ambon montrant la situation des principales unités ophiolitiques (modifié d'après Tjokrosapoetro and Budhitrisna [1982]).*

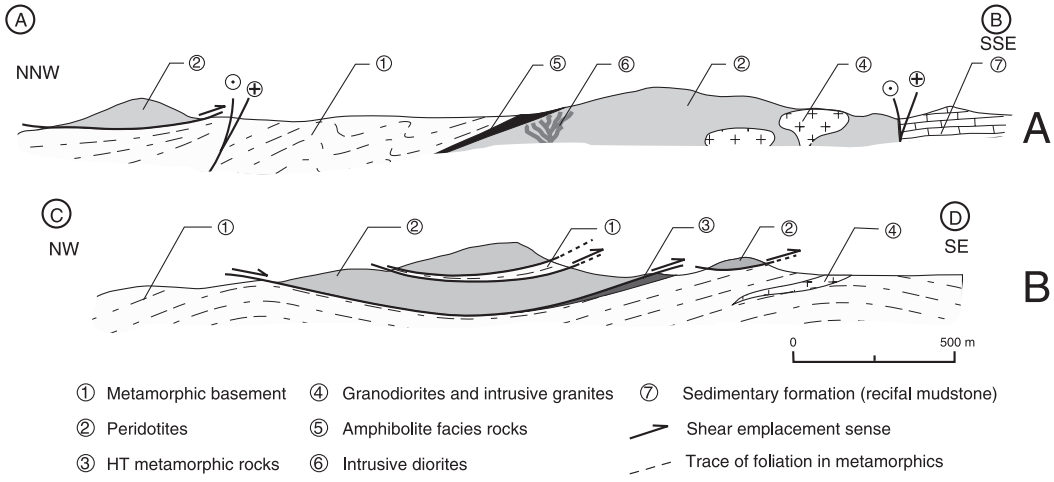

FIG. 2. – Simplified cross-sections of A) Kaibobo and B) Ariate areas on the Seram island.
FIG. 2. – *Coupes simplifiées* A) *de la région de Kaibobo et* B) *de Ariate sur l'ile de Seram.*

PETROGRAPHICAL DATA

The plagioclase lherzolites and the Cpx-rich harzburgites present granoblastic to porphyroclastic textures. Their serpentinisation ranges from ~2 % to ~25 %. The Pl-lherzolites have modal compositions ranging between 80.5-81.5 % Ol+Serp, 8.0-9.0 % Opx, 4.0-5.3 % Cpx, 0.9-1.3 % Sp and 2.5-5.5 % Pl (tabl. I). These rocks are characterized by high olivine contents and by the presence of interstitial plagioclase closely associated with the pyroxenes and, locally, with spinel. In the Cpx-rich harzburgites, the modal phase content is 84.0-87.5 % Ol+Serp, 6.6-9.0 % Opx, 3.0-3.5 % Cpx, 0.6-1.1 % Sp and 0.7-2.2 % Pl (tabl. I). Like the Pl-lherzolites, they are particularly rich in olivine. Most of the Cpx-free harzburgites present typical porphyroclastic textures except for a few samples that are mylonites with strongly elongated Opx. They have modal compositions of 83.5-85.5 % Ol+Serp, 12-15 % Opx, 0.4-0.9 % Sp and traces of plagioclase (<0.5 %).

The websterites are slightly altered (1.04<L.O.I<5.23 % – table II) and present isogranular to mylonitic textures. They contain 20 % Ol, 20 % Opx, 30-40 % Cpx, 10-15 % Pl (Pl-poor) to 15-30 % Pl (Pl-rich) and rare Sp (<0.5 %). In these rocks, the plagioclase phase is associated with the clinopyroxene in the Pl-poor websterites and with spinel and clinopyroxene phases in the Pl-rich websterites, forming locally well-developed symplektitic structures.

Most of the gabbros are fresh to slightly altered (0.15<L.O.I<3.16 wt % – tables II). The olivine-bearing gabbros display a typical mesocumulate texture. Others present coarse-grained isotropic adcumulate to pegmatitic textures (e.g. ABN1b, ABN1c and ABN1k) and contain poikelitic amphiboles (hornblende to tchermatic-hornblende).

Lavas are very fresh to altered (0.95<L.O.I<4.05 wt % – tables III), undeformed and have mostly typical sub-aphyric/intersertal to porphyric textures with plagioclase, clinopyroxene (augite) and primary amphibole (tchermakitic-hornblende – TiO_2>3 %) phenocrysts. Sample ABN1a is rather rich amphibole (hornblende).

MINERAL COMPOSITION OF ULTRAMAFIC ROCKS

Mineral compositions have been obtained with a CAMEBAX SX50 (Microsonde Ouest, Brest) using silicate standards (albite, wollastonite, orthoclase, vanadine) for calibration of Na, Si, Ca, K and oxide standards for calibration of Fe, Mn, Al and Ni. For analyses, the accelerating voltage was 15Kv, the beam current 15nA and the counting time between 6 and 25s depending on the element.

Olivine from Pl-lherzolites have Mg# (Mg#=100*[Mg/Mg+Fe]) between 89 to 90 %. These values slightly increase in the Cpx-rich harzburgites (90-91 %) and in the Cpx-free harzburgites (90-92 %), in agreement with their respective Ni (1000*Ni) concentrations (respectively 4.6, 4.9 and 5.4, in average) (fig. 3A). The refractory nature of olivine is inconsistent with the orthopyroxene Cr# contents (Cr#=2*Cr/[Cr+Al-Na]) which slightly increase from the Cpx-free harzburgites ($Cr\#_{(Opx)}$=0.27) to the Cpx-rich harzburgites ($Cr\#_{(Opx)}$=0.34) and the Pl-lherzolites ($Cr\#_{(Opx)}$=0.37). It is also inconsistent with the spinel Cr# (Cr#=[Cr/(Cr+Al)]) content (respectively 0.40, 0.48, 0.51 in average – fig. 3B) which increases from the Cpx-free harzburgites to the Pl-lherzolites, as also their Ti contents (fig. 3C). This indicates that the plagioclase formed by sub-solidus reequilibration reaction when the rocks passed in the plagioclase field during their ascent [Kornprobst and Tabit, 1988 ; Li, 1991 ; Cornen *et al.*, 1996 ; Charpentier, 2000]. Textural data show that, in our case, the plagioclase formation occurred after the formation of Cpx-free harzburgite.

BULK ROCKS CHEMICAL DATA

Major and trace elements including rare-earths have been analysed in 44 samples, including 15 peridotites, 1 orthopyroxenite, 9 websterites, 5 gabbros and 14 lavas (see tables I, II and III).

TABLE I. – Selected bulk-rock chemistry of the Seram-Ambon peridotites and pyroxenites. Pl-Lz.= plagioclase-bearing lherzolite, Sp-Lz.= Cpx-rich spinel harzburgite, Hz.= Cpx free harzburgite. Major elements data in wt %, minor elements data in ppm and rare-earth elements in ppb. The selected modal phase compositions have been obtained by image analysis.

TABL. I. – *Analyses chimiques sur roches totales de roches ultramafiques représentatives des îles de Seram-Ambon.* Pl-Lz.= *lherzolite à plagioclase,* Sp-Lz.= *harzburgite à spinelle riche en Cpx*, Hz.= *harzburgite sans Cpx. Les éléments majeurs sont donnés en poids d'oxydes, les éléments de transition en ppm et les terres rares en ppb. Les compositions modales des péridotites ont été obtenues par analyse d'images.*

N° Rocks	SM10a Pl-Lz.	ABN5c Pl-Lz.	ABN5d Pl-Lz.	ABN5e Pl-Lz.	KBB29 Pl-Lz.	KBB11 Pl-Lz.	ABN12a Cpx-rich harz.	ABN4a Cpx-rich harz.	KBB38 Cpx-rich harz.	KBB18c Cpx-rich harz.	KBB 17b Cpx-rich harz.	KBB41 Cpx-rich harz.	KBB 46c Cpx-free harz.	KBB 19b Cpx-free harz.	KBB 19c Cpx-free harz.	KBB 46e Ortpx.
Ol %	78.5		71.0	73.0			84.0	72.0			88.0		82.0	79.0	77.7	
Opx %	8.2		8.0	9.0			8.2	9.0			6.7		13.0	12.3	15.0	
Cpx %	4.0		5.3	4.6			3.5	3.0			/		/	/	/	
Sp %	1.3		1.0	0.9			1.1	0.6			0.9		0.9	0.8	0.4	
Pl %	5.5		3.2	2.5			2.2	0.7			0.9		0.2	0.3	0.5	
Serp %	2.0		12.5	10.2			3.8	15.0			3.5		3.2	7.5	6.0	
SiO2	43.50	44.20	43.00	43.10	40.60	40.20	43.30	42.50	39.80	44.00	42.00	42.50	43.00	43.00	44.50	52.80
TiO2	0.10	0.09	0.09	0.09	0.10	0.10	0.05	0.04	0.04	0.03	0.05	0.08	0.03	0.02	0.02	0.03
Al2O3	3.20	2.55	3.93	3.06	2.60	2.57	2.24	1.18	1.01	1.58	1.88	2.44	1.03	1.90	2.05	1.25
Fe2O3	9.03	8.84	8.10	8.30	8.45	7.90	8.15	7.80	8.70	7.84	7.91	8.25	8.80	8.55	8.05	6.85
MnO	0.13	0.13	0.12	0.12	0.13	0.12	0.10	0.11	0.12	0.11	0.12	0.12	0.13	0.13	0.12	0.12
MgO	39.70	40.00	35.80	36.50	36.80	35.60	39.60	40.50	35.00	36.85	40.65	35.60	42.40	40.40	39.00	36.20
CaO	3.42	2.33	2.38	2.28	2.16	1.97	2.55	1.03	0.89	1.20	1.71	2.20	0.62	1.25	1.85	0.72
Na2O	0.19	0.22	0.37	0.25	0.04	0.10	0.28	0.05	0.03	0.07	0.07	0.08	0.03	0.12	0.10	0.02
K2O	0.00	0.02	0.00	0.01	0.00	0.01	0.02	0.01	0.00	0.01	0.00	0.00	0.00	0.01	0.00	0.00
P2O5	0.02	0.02	0.02	0.02	0.02	0.01	0.01	0.01	0.02	0.01	0.01	0.02	0.01	0.01	0.01	0.01
L.O.I	-0.12	1.51	5.63	5.74	9.05	10.73	3.63	6.19	13.63	7.23	4.61	7.94	2.82	3.41	2.35	1.37
Total	99.17	99.91	99.44	99.47	99.95	99.31	99.93	99.42	99.23	98.93	99.02	99.23	98.87	98.80	98.05	99.37
ppm																
Ti	528	485	503	498	469	495	270	180	128	116	191	194	56	32	48	78
V	72	56	57	62	68	63	48	40	52	52	47	64	32	47	58	32
Cr	2200	1560	1360	1670	2 550	2 400	1800	1600	3 100	2690	2800	2700	2650	2800	3250	8500
Co	108	95	85	88	98	100	94	92	112	110	106	100	115	103	104	72
Ni	2100	2080	1860	1880	1 900	2 000	2160	2130	2 350	2250	2220	2250	2380	2580	2200	1200
Cu	24	17	31	16	16	21	2	9	3	10	15	5	5	6	5	2
Zn	40	36	42	38	22	20	24	32	16	13	26	6	31	28	23	17
ppb																
La	18	89	69	62	79	43	91	10	13	118	305	113	6	19	31	5
Ce	144	320	333	286	278	209	227	56	53	245	600	246	11	38	59	8
Pr	49	66	71	65	62	58	37	17	12	25	58	34	3	5	5	1
Nd	363	429	478	471	415	389	201	116	107	101	202	159	15	25	20	11
Sm	197	173	239	214	183	182	86	57	40	36	50	57	8	5	8	5
Eu	89	78	105	83	70	81	42	23	18	15	22	26	4	2	2	3
Gd	322	310	398	325	297	316	159	97	69	61	99	93	22	17	22	10
Tb	70	59	76	68	59	59	34	21	13	13	19	18	6	5	4	2
Dy	497	401	548	486	407	409	241	144	94	99	153	130	38	39	50	19
Ho	110	95	128	112	95	91	55	33	22	24	34	30	10	13	13	4
Er	321	285	358	335	282	278	187	106	70	79	113	92	36	42	46	14
Tm	49	43	57	49	41	41	28	15	11	12	15	13	6	8	/	2
Yb	317	298	383	330	289	277	197	108	72	90	105	96	47	48	51	13
Lu	47	45	55	54	44	42	30	16	12	14	16	15	8	10	8	3

TABLE II. – Selected bulk-rock chemistry of websterites and gabbros from Seram-Ambon islands. Major element data in wt %, minor and trace element data in ppm.

TABL. II. – *Analyses chimiques sur roches totales de quelques webstérites et gabbros représentatifs des îles de Seram et de Ambon. Les éléments majeurs sont donnés en poids d'oxydes, les éléments de transition et en traces en ppm.*

N° Rocks	KBB 19e Websterite Type 1	KBB 19f Websterite Type 1	ABN14d Websterite Type 1	ABN14f Websterite Type 1	ABN1d Websterite Type 2	ABN1l Websterite Type 2	ABN10b Websterite Type 2	KL2a Websterite Type 3	KL2b Websterite Type 3	ABN1i Gabbro Group 1	KL1g Gabbro Group 1	ABN1k Gabbro Group 2	ABN1b Gabbro Group 2	ABN1c Gabbro Group 2
SiO2	46.80	46.75	44.50	43.50	47.20	48.00	46.80	51.50	46.70	50.00	48.70	48.80	48.00	47.00
TiO2	0.25	0.29	0.13	0.13	0.19	0.20	0.35	0.17	0.14	0.47	0.31	0.12	0.11	0.10
Al2O3	9.00	7.98	14.25	11.55	11.20	10.50	12.10	7.18	15.50	6.48	18.60	14.15	14.80	15.20
Fe2O3	6.50	6.86	5.25	6.55	8.20	8.10	7.52	3.52	5.94	8.90	6.15	7.95	8.25	10.15
MnO	0.15	0.15	0.11	0.12	0.17	0.18	0.18	0.06	0.12	0.15	0.10	0.17	0.17	0.21
MgO	18.10	21.15	18.00	21.10	18.60	18.10	18.00	16.50	17.35	17.20	8.72	13.40	13.65	15.35
CaO	15.70	12.90	12.00	10.45	11.40	12.60	9.60	19.50	12.34	13.70	13.70	10.66	10.68	10.65
Na2O	0.37	0.36	0.76	0.66	0.77	0.79	0.97	0.75	0.52	0.68	1.86	1.40	1.44	1.40
K2O	0.03	0.02	0.04	0.02	0.04	0.05	0.03	0.09	0.22	0.05	0.07	0.04	0.04	0.00
P2O5	0.01	0.02	0.02	0.02	0.02	0.02	0.02	0.02	0.04	0.02	0.04	0.02	0.02	0.03
L.O.I	2.96	2.83	4.43	5.23	2.51	2.01	4.15	1.04	0.58	2.54	1.96	2.89	3.16	0.15
Total	99.87	99.30	99.49	99.33	100.30	100.55	99.72	100.33	99.45	100.19	100.21	99.60	100.32	100.24
ppm														
Ti	1952	2384	617	621	1092	1052	1954	881	759	2574	1953	655	664	586
V	545	400	122	110	245	310	285	95	72	405	136	325	325	330
Cr	1580	2650	1085	2625	730	920	800	2850	1320	650	550	580	595	750
Co	56	61	47	60	51	46	46	34	48	46	32	37	40	48
Ni	300	572	620	710	620	410	840	730	425	1200	110	268	290	195
Cu	72	65	11	1	94	30	89	29	13	99	70	3	1	29
Zn	40	43	26	42	34	29	24	14	13	34	41	35	40	52
ppm														
Sc	64	52	36	29	40	46	46	10	21	30	33	35	40	47
Rb	1.36	0.75	0.27	0.27	0.33	0.31	0.28	1.15	3.57	1.57	1.14	0.33	0.46	0.14
Sr	26	47	61	21	25	33	45	130	74	39	123	22	22	15
Y	5.26	5.02	3.44	3.51	9.38	10.53	13.37	1.07	3.09	14.99	11.05	7.18	7.72	6.71
Zr	3.34	4.13	2.96	4.04	3.01	3.16	2.53	7.10	10.79	9.104	14.70	1.38	1.58	0.93
Nb	0.04	0.05	0.04	0.05	0.02	0.01	/	1.56	0.42	0.01	0.25	/	/	/
Cs	0.26	0.19	0.03	0.03	0.16	0.06	0.09	0.10	0.11	0.24	0.02	0.15	0.20	0.05
Ba	0.48	0.40	0.52	0.42	0.86	0.57	0.83	7.35	15.82	0.58	9.36	0.66	0.59	0.76
La	0.25	0.32	0.31	0.29	0.06	0.02	0.04	3.28	1.58	0.99	0.82	0.05	0.05	0.03
Ce	0.63	0.90	0.87	0.89	0.15	0.07	0.20	8.74	4.16	2.73	2.77	0.15	0.18	0.10
Pr	0.10	0.16	0.13	0.13	0.04	0.03	0.06	1.07	0.53	0.48	0.47	0.04	0.04	0.03
Nd	0.93	0.91	0.75	0.70	0.44	0.39	0.50	3.73	1.98	2.75	2.75	0.25	0.29	0.23
Sm	0.33	0.44	0.27	0.30	0.49	0.54	0.42	0.79	0.63	1.19	1.08	0.13	0.11	0.10
Eu	0.19	0.21	0.16	0.16	0.24	0.26	0.28	0.17	0.19	0.63	0.52	0.11	0.09	0.08
Gd	0.63	0.72	0.51	0.40	1.36	1.13	1.04	0.37	0.52	2.74	1.64	0.43	0.34	0.34
Tb	0.13	0.14	0.09	0.09	0.25	0.23	0.27	0.05	0.10	0.46	0.30	0.12	0.10	0.10
Dy	0.96	0.98	0.64	0.66	1.69	1.85	2.20	0.28	0.65	3.07	2.05	1.09	1.05	0.95
Ho	0.22	0.21	0.15	0.15	0.44	0.46	0.52	0.05	0.14	0.64	0.48	0.30	0.31	0.28
Er	0.65	0.56	0.44	0.43	1.30	1.47	1.70	0.13	0.37	1.99	1.26	1.07	1.05	0.99
Tm	0.08	0.09	0.06	0.07	0.20	0.23	0.24	0.02	0.05	0.28	0.19	0.18	0.18	0.18
Yb	0.55	0.53	0.41	0.42	1.81	1.46	1.53	0.10	0.34	2.02	1.18	1.36	1.25	1.29
Lu	/	/	0.06	0.06	0.39	0.22	0.21	0.02	0.05	0.31	0.17	0.23	0.19	0.23
Hf	0.11	0.18	0.12	0.13	0.10	0.09	0.14	0.38	0.34	0.348	0.48	0.14	/	0.11
Th	0.01	0.01	0.01	0.01	/	0.01	/	0.15	0.10	0.003	0.027	0.005	/	0.007
U	/	/	/	/	/	/	/	0.05	0.03	0.001	0.010	/	/	/

TABLE III. – Selected bulk-rock chemistry of back-arc basin basalts (BABB) and island arc-tholeiites (IAT) from Seram-Ambon islands. Major element data in wt %, minor and trace element data in ppm.

TABL. III. – *Analyses chimiques sur roches totales de quelques basaltes arrière-arc et tholéiites d'arc représentatifs des îles de Seram et de Ambon. Les éléments majeurs sont donnés en poids d'oxydes et les éléments de transition et en traces en ppm.*

N°	ABN1a	ABN1e	ABN6f	ABN6e	ABN6d	ABN5b	ABN6c	SM16d	SM15c	SM16c	ABN10a	ABN1j	ABN6a	KL15a
Rocks	BABB	BABB	BABB	BABB	BABB	BABB	BABB	BABB	BABB	BABB	IAT	IAT	IAT	IAT
Ages (Ma)	19.3						15	19.7				15.3	8.9	
SiO2	44.60	46.50	48.00	50.60	51.50	51.50	51.50	52.80	53.70	58.30	44.80	48.50	48.60	53.50
TiO2	1.00	1.07	0.83	0.74	0.71	0.72	0.74	0.80	0.66	0.86	0.58	0.55	0.69	0.50
Al2O3	12.50	17.00	18.25	15.96	15.65	16.40	16.10	19.05	16.30	15.80	15.95	21.40	17.50	14.30
Fe2O3	10.35	8.75	5.92	8.50	8.20	7.90	8.05	7.55	7.50	8.16	9.38	2.62	5.65	7.35
MnO	0.21	0.15	0.12	0.14	0.14	0.14	0.14	0.13	0.13	0.08	0.20	0.06	0.15	0.12
MgO	15.30	10.30	11.50	9.05	9.10	8.30	8.65	5.85	7.05	4.44	9.45	8.75	11.80	10.00
CaO	10.20	11.10	12.30	10.96	10.98	11.15	10.45	10.20	9.90	7.20	14.35	15.20	11.95	10.25
Na2O	1.47	2.25	1.84	2.32	2.63	2.64	2.79	2.03	2.51	1.80	1.12	0.96	0.82	1.15
K2O	0.15	0.13	0.18	0.05	0.06	0.06	0.11	0.09	0.05	0.05	0.10	0.23	0.79	0.06
P2O5	0.09	0.11	0.08	0.07	0.07	0.07	0.07	0.08	0.07	0.10	0.07	0.18	0.07	0.06
L.O.I	4.05	2.74	1.65	0.74	0.80	0.95	1.16	1.86	1.56	2.59	3.82	1.36	2.20	1.88
Total	99.92	100.10	100.67	99.13	99.84	99.83	99.76	100.44	99.43	99.38	99.82	99.81	100.22	99.17
ppm														
Ti	6708	7289	4622	4616	4623	5223	5270	5290	5755	6842	3669	5949	4556	3833
V	243	199	228	228	223	244	261	277	224	232	275	237	252	209
Cr	787	507	577	457	430	352	195	79	436	9	265	535	526	363
Co	55	44	39	39	38	36	29	27	35	28	36	28	39	37
Ni	1403	441	265	155	151	158	133	84	144	49	113	508	257	194
Cu	14	1	18	36	40	57	142	20	94	12	11	6	5	64
Zn	58	2	34	41	47	41	47	48	110	27	63	13	28	52
ppm														
Sc	37	33	37	37	36	36	34	37	34	31	43	28	41	34
Rb	0.84	2.52	5.55	0.48	0.43	0.36	0.35	0.82	2.82	4.11	0.51	2.49	19.59	0.69
Sr	160	252	170	155	107	146	146	132	143	143	512	333	156	130
Y	26	21	20	17	17	18	16	16	17	23	15	24	20	13
Zr	51	46	34	30	30	24	33	22	32	48	28	20	24	33
Nb	0.89	1.05	0.43	0.38	0.37	0.50	0.84	0.96	0.35	1.30	5.34	11.16	0.77	0.78
Cs	0.31	0.66	0.70	0.05	0.02	0.01	0.02	0.05	0.59	0.60	0.02	0.28	0.82	0.03
Ba	22	51	58	38	58	31	32	18	62	16	32	26	167	35
La	2.90	3.35	2.40	1.73	1.65	2.13	2.61	2.69	1.77	2.39	21.83	16.57	6.54	3.10
Ce	7.04	10.37	6.51	5.26	5.12	6.21	6.95	7.46	5.69	6.95	37.45	31.17	14.40	7.55
Pr	1.34	1.78	1.09	0.97	0.93	1.08	1.08	1.15	1.04	1.16	3.90	3.88	1.95	1.14
Nd	7.69	9.22	6.35	5.43	5.28	5.87	5.69	5.85	5.76	6.10	13.91	16.54	8.98	5.28
Sm	2.70	2.86	2.27	1.87	1.90	2.08	1.82	1.82	2.06	2.27	2.55	3.86	2.63	1.63
Eu	1.01	1.12	0.84	0.83	0.75	0.77	0.71	0.71	0.80	0.78	1.08	0.68	0.94	0.55
Gd	3.73	3.69	3.25	2.75	2.72	2.80	2.47	2.42	2.88	3.13	2.73	4.22	3.49	2.04
Tb	0.66	0.62	0.57	0.49	0.48	0.50	0.46	0.44	0.50	0.61	0.46	0.70	0.58	0.36
Dy	4.49	4.09	3.72	3.23	3.25	3.47	2.87	2.89	3.28	4.12	2.88	4.51	3.84	2.56
Ho	0.97	0.88	0.81	0.69	0.68	0.72	0.63	0.61	0.74	0.88	0.63	0.95	0.81	0.55
Er	2.80	2.41	2.28	1.98	2.06	2.08	1.81	1.89	2.02	2.58	1.81	2.77	2.38	1.54
Tm	0.41	0.34	0.35	0.30	0.31	0.29	0.26	0.27	0.30	0.37	0.27	0.40	0.35	0.24
Yb	2.51	2.16	2.22	1.92	1.86	1.98	1.78	1.85	1.96	2.52	1.81	2.61	2.22	1.55
Lu	0.39	0.29	0.33	0.28	0.27	0.29	0.26	0.26	0.30	0.35	0.28	0.39	0.34	0.24
Hf	1.81	1.48	0.96	0.96	1.17	0.81	1.17	0.98	0.86	1.60	0.95	0.69	0.93	1.11
Ta	0.06	0.08	0.04	0.03	0.02	0.03	0.08	0.06	0.04	0.09	0.34	0.66	0.05	0.05
Th	0.38	0.18	0.33	0.33	0.32	0.39	0.42	0.59	0.29	0.65	4.12	4.02	0.54	0.54
U	0.07	0.04	0.12	0.13	0.19	0.12	0.18	0.15	0.15	0.29	0.49	1.13	0.17	0.18

Analytical procedure

Bulk rock major and minor elements have been analysed by Inductively Coupled Plasma Atomic Emission Spectrometry (ICP-AES) at University of Brest using Cotten et al. [1995] procedure for sample preparation and acid dissolution. Associated geostandards are AC-E, BE-N, KB-2 and MICA-Fe. Relative standard deviations are ca. 2 % for major elements and <5 % for trace elements analysed by this technique.

Trace elements have been analyzed by Inductively Coupled Plasma Mass Spectrometry (ICP-MS) at University of Toulouse. For most of the samples, acid dissolution and further evaporation have been performed in a CEM microwave oven following the procedure described by Benoit *et al.* [1996]. The final solution is HNO3 0.37N diluted 300 times (peridotites, websterites and gabbros) and 1000 times (basalts) for acid-digested samples. ICP-MS is a Perkin Elmer(ELAN 5000 equiped with a classical cross flow nebulizer and a Scott spray chamber. Reproducibility and accuracy of the whole procedure (sample dissolution and analysis) were checked through the analysis of geostandards BE-N, JP1, UBN, PMS.

Peridotites

In agreement with their modal compositions and phase chemistry, the major element compositions of peridotites display distinctive characteristics compared to the primitive mantle (tab. I). From the Pl-lherzolites to the harzburgites, the MgO contents remain nearly constant at ca. 38.20 wt %. The Pl-lherzolites tend to be enriched in CaO (2.42 wt % in average) and in Al_2O_3 (3.00 wt % in average) compared to the Cpx-rich harzburgites (1.60 and 1.72 wt %, respectively) and the harzburgites (1.10 and 1.56 wt %, respectively), in agreement with their respective modal content of plagioclase.

The chondrite-normalized rare-earth element (REE) abundances of the Pl-lherzolites display regular and homogeneous patterns (fig. 4A). From heavy rare-earth elements (HREE) to middle rare-earth elements (MREE), these peridotites show nearly flat patterns ($(Lu/Eu)_N$=1.4 in average)

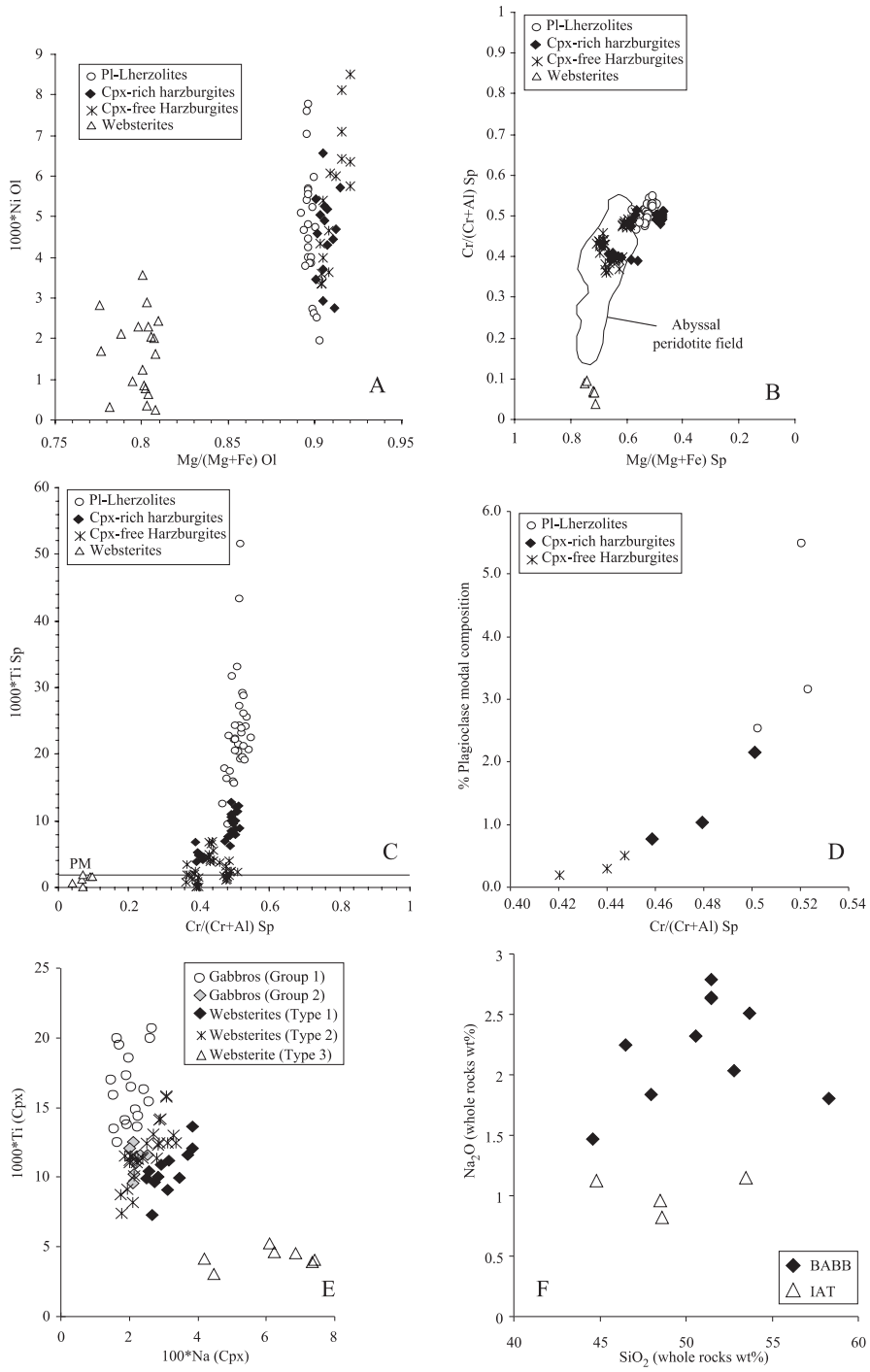

FIG. 3. – A) olivine : 1000*Ni versus Mg#, B) spinel : Cr# versus Mg#, C) spinel : 1000*Ti versus Cr#, D) plagioclase modal composition (in %) versus Cr# of spinel from Pl-lherzolites, Cpx-rich harzburgites and Cpx-free harzburgites, E) Cpx : 1000*Ti versus 100*Na in gabbros and websterites, F) Na_2O wt $\%_{(WR)}$ versus SiO_2 wt $\%_{(WR)}$ in BABB and IAT.

FIG. 3. – A) *olivine : 1000*Ni versus Mg#*, B) *spinelle : Cr# versus Mg#,* C) *spinelle : 1000*Ti versus Cr# du spinelle*, D) *composition modale (en %) du plagioclase versus Cr# spinelle des lherzolites à plagioclase, des harzburgites riches en Cpx et des harzburgites sans Cpx*, E) *Cpx : 1000*Ti versus 100*Na des gabbros et websterites*, F) *Na_2O $\%_{(RT)}$ versus SiO_2 $\%_{(RT)}$ dans les basaltes arrière-arc et les tholéiites d'arc.*

at ca. 1.7 times chondritic values. But they also display depletions in light rare-earth elements (LREE) relative to MREE ($(La/Eu)_N$=0.2 in average). The Cpx-rich harzburgites (fig. 4B) display low rare-earth element (REE) concentrations relative to chondritic values (Lu_N=0.7, Eu_N=0.4 in average). However, most of them show a slight enrichment in LREE, well marked by the La-Eu segment ($(La/Eu)_N$=1.6 in average).

By comparison, Cpx-free harzburgites show very distinctive REE patterns (fig. 4C), with very low HREE (0.1-0.3 times chondrites) and a slight depletion toward the MREE ($(Lu/Eu)_N$=7.0 in average). Such low concentrations are typical of high residual mantle peridotites [Saunders and Tarney, 1984 ; Bodinier *et al.*, 1990 ; Kelemen *et al.*, 1990 ; Maury *et al.*, 1992 ; Parkinson *et al.*, 1992]. Note that some of the Cpx-rich harzburgites (KBB17b and

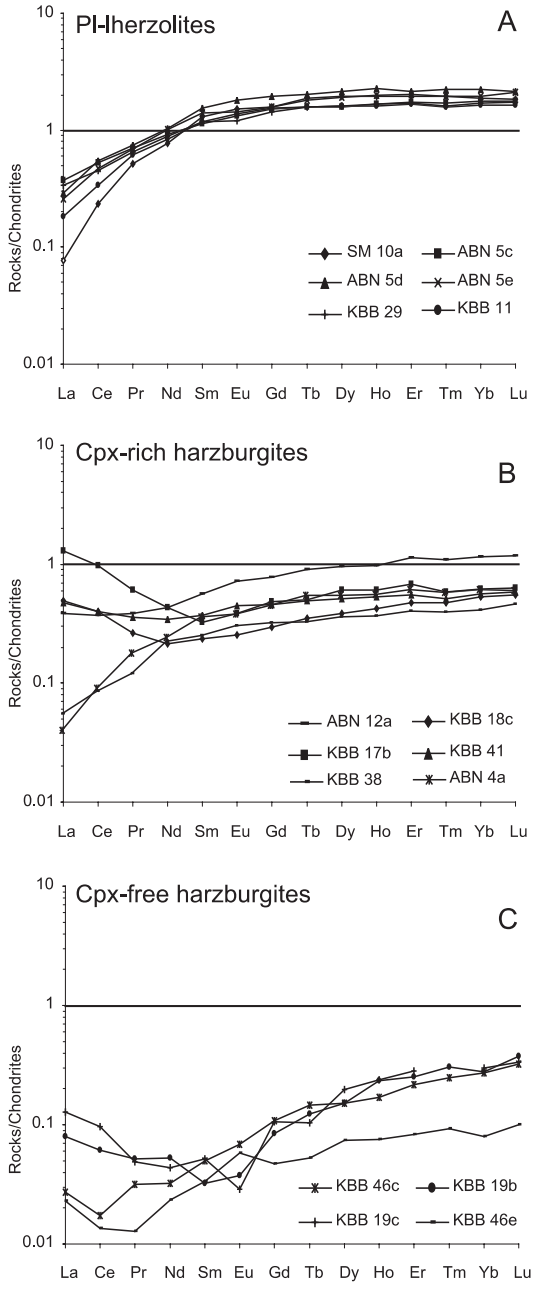

FIG. 4. – Chondrite-normalized rare-earth elements for the Seram-Ambon peridotites. A) Pl-lherzolites, B) Cpx-rich harzburgites and D) Cpx-free harzburgites. Normalization values from Sun and McDonough [1989].
FIG. 4. – *Spectres de terres-rares des péridotites de Seram-Ambon normalisés aux chondrites.* A) *lherzolites à plagioclase,* B) *harzburgites riches en Cpx et* D) *harzburgites sans Cpx. Valeurs de normalisation d'après Sun et McDonough [1989].*

Kbb18c) show significative LREE enrichments ($(La/Sm)_N$>2), which imply that metasomatism process occurred in these rocks after a partial melting event [Wiechert *et al.*, 1996].

Gabbros and websterites

Composition of gabbros and websterites is given in table II. In gabbros, MgO varies from 17.35 to 8.72 wt %. Al_2O_3 increases from the meso-cumulate olivine-gabbros (14.15 wt %) to the adcumulate isotropic ones (18.60 wt %), like TiO_2 (0.12 to 0.31wt %, respectively) as expected for fractional

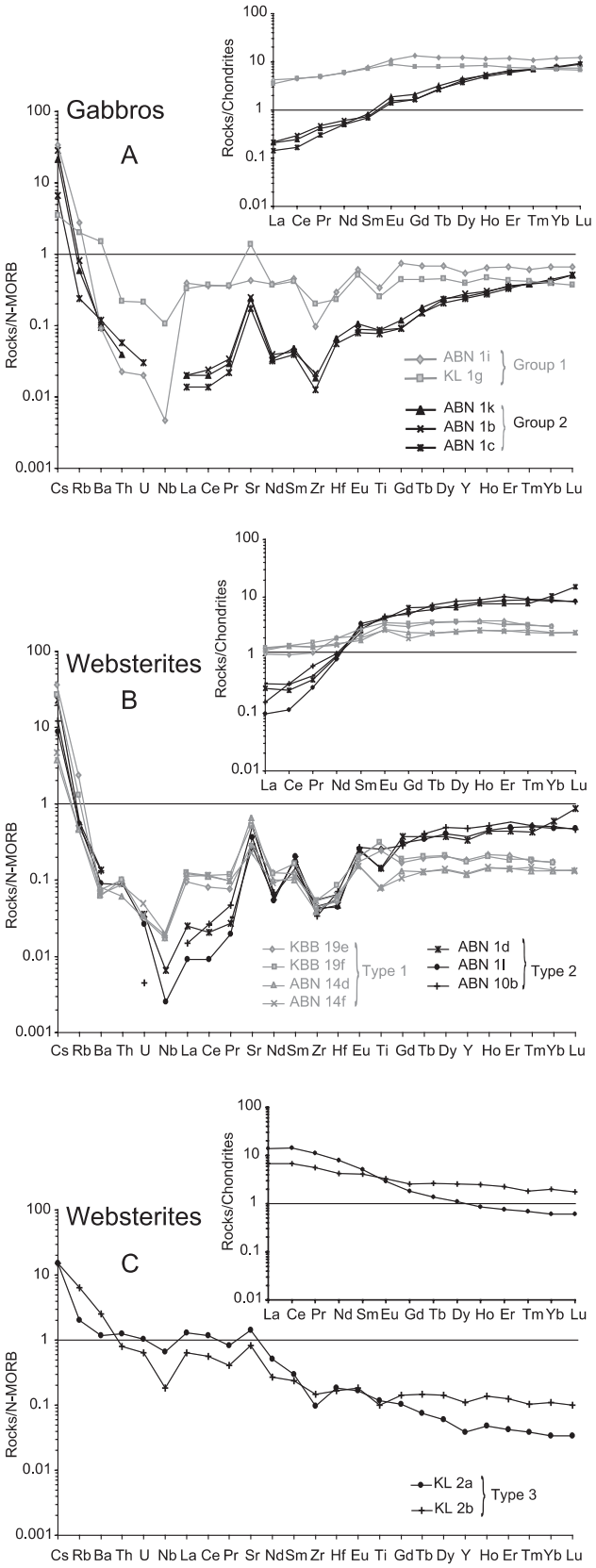

FIG. 5. – Chondrite-normalized REE patterns and N-MORB-normalized rare-earth elements for A) group 1 and group 2 gabbros, B) type 1 and type 2 websterites and C) type 3 websterites. Normalization values from Sun and McDonough [1989].
FIG. 5. – *Spectres de terres-rares normalisés aux chondrites et spectres multi-éléments normalisés aux N-MORB pour* A) *les gabbros des groupes 1 et 2,* B) *les websterites de type 1 et 2 et* C) *les websterites de type 3. Valeurs de normalisation d'après Sun et McDonough [1989].*

crystallization. Their chondrite-normalized REE patterns [Sun and McDonough, 1989] show two distinct groups with regular shapes (fig. 5A). The group 1 gabbros (ABN1i and KL1g) have 6-10 times chondritic values for MREE to HREE, shows nearly flat REE patterns ($0.38<(La/Yb)_N<0.65$) and are slightly depleted in LREE. The group 2 gabbros (ABN1k, ABN1b and ABN1c) are in marked contrast by a strong depletion in the LREE relative to the HREE ($0.02<(La/Yb)_N<0.04$).

The websterites have a moderate compositional range, with a MgO between 15.50 and 21.50 wt %, and Al_2O_3 between 7.18 and 15.50 wt %. Like the gabbros, they also display distinctive REE patterns which allows to define 3 types of websterites (fig. 5B-5C). The type 1 websterites (KBB19e, KBB19f, ABN14d and ANB14f) are similar to group 1 gabbros with, however, lower REE concentrations (2-3 times the chondrites). Type 2 websterites (ABN1d, ABN1l and ANB10b) are more enriched in HREE and MREE (5 to 9 times the chondritic values) and more LREE-depleted (La_N=0.1-0.2). The type 3 websterites (KL2a and KL2b) are very distinctive from others owing to their very low HREE concentrations (0.6 to 1.8 times the chondrites) and very high LREE enrichment ($3.40<(La/Yb)_N<24.00$ – fig. 5C). Their N-MORB normalized trace element concentrations are marked by enrichment in large ion lithophile elements (LILE) and by slight HFSE-depletions (Zr, Nb and Y).

Volcanic rocks

All the studied volcanic rocks are characterized by a moderate range of SiO_2 content, that varies between 46.60 and 58.30 wt % (tabl. III). They are marked by high Al_2O_3 (16.60 wt %, in average) and by low TiO_2 and K_2O (0.75 and 0.15 wt %, in average respectively), which is typical of low-K orogenic basalts. Samples ABN1a, ABN1e, ABN6f, ABN6a and KL15a have chemical compositions typical of primary melts according to their high MgO contents (>10 wt %) and Ni and Cr concentrations (up to 265 and 500 ppm, respectively).

Despite these common chemical features, some volcanic rocks have higher Na_2O concentrations, typical of MORB values (2.23 wt % in average – fig. 3F), than expected from their SiO_2 contents. According to their low TiO_2 and high Al_2O_3 contents, these rocks likely generated in a back-arc basin setting (BABB) [Saunders and Tarney, 1984 ; Monnier *et al.*, 1995]. On the other hand, other basalts with lower Na_2O concentrations (<1.15 wt %) are typical of island arc-tholeiites (IAT).

The chondrite-normalized REE patterns of BABB are MORB-like ($0.55<(La/Sm)_N<0.96$ – fig.6B). Their extended N-MORB-normalized diagrams are characterized by very high $(La/Nb)_N$ ratio (4.20 in average), which strongly suggests a subduction zone environment for their origin [Saunders and Tarney, 1984 ; Monnier *et al.*, 1995]. Moreover, these rocks have high U and Th concentrations (0.12 and 0.34 ppm in average, respectively) giving high Th/Nb ratios (0.62 in average) closely similar to those of back-arc basin basalts generated during rifting of a continental margin crust [Auzende *et al.*, 1990 ; Eissen *et al.*, 1998].

The chondrite-normalized REE patterns of IAT (fig. 6A) are characterized by moderate to high enrichments in LREE (20 to 100 times the chondritic values). Their extended

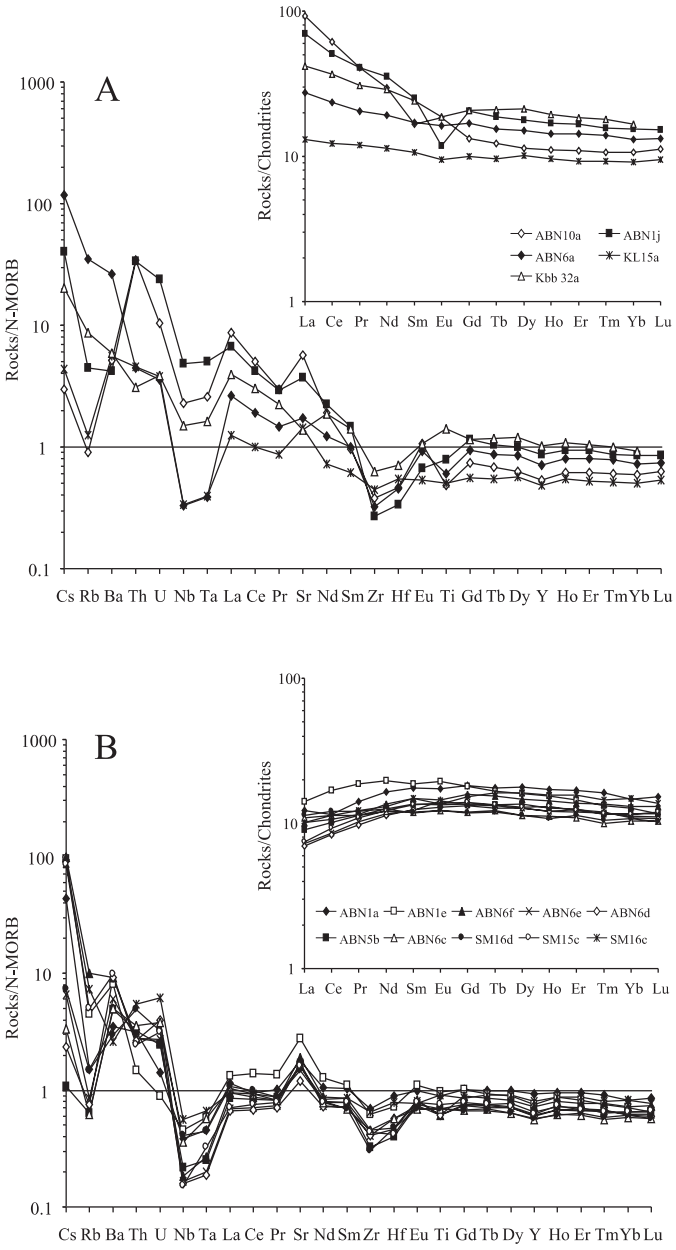

FIG. 6. – Chondrite-normalized REE patterns and N-MORB-normalized rare-earth elements for A) the back-arc basin basalts and B) the arc-tholeiites. Normalization values from Sun and McDonough [1989].
FIG. 6. – *Spectres de terres-rares normalisés aux chondrites et spectres multi-éléments normalisés aux N-MORB pour* A) *les basaltes arrière-arc et* B) *les tholéiites d'arc. Valeurs de normalisation d'après Sun et McDonough [1989].*

N-MORB-normalized diagrams show an enrichment of LILE relative to REE and typical HFSE depletions (Nb, Ta, Zr and Y) as shown by their high $(La/Nb)_N$ ratio (3.89 in average) which is closely similar to the BABB. This is also shown by the Th/Nb ratios (0.56 in average).

GEOCHRONOLOGICAL DATA

Analytical procedure

Whole rock $^{40}K/^{40}Ar$ ages have been done at University of Brest on the most representative lavas from both the BAB and IAT series. For whole rocks dating, samples were

crushed and sieved to 315-160 μm grain size and then cleaned with distilled water. This fraction was used (1) for argon extraction under high vacuum by HF heating and (2) after reduction to a powder for potassium analysis by atomic absorption spectrometry. Ages calculation were carried out using the constants recommended by Steiger and Jäger [1977] with a one Sigma error calculated according to Mahood and Drake [1982]. Chronostratigraphic significance of dates refers to the geological time scale [Odin, 1994].

Samples affected by obvious hydrothermal alteration were exclude from the data set. Except for Cs, Rb (and for Ba, not used to plot), there is no correlation between the alteration index (L.O.I) and the major and trace element content of rocks (e.g. K_2O, Na_2O, Sr, Th or U).

Results

Three back-arc basalts and two island-arc tholeiites have been dated. Radiochronological results are presented in table IV, with the most characteristic parameters of the measurements, among them : the $^{40}Ar^*$ – radiogenic argon^{40}, the percentage of $^{40}Ar^*$ versus the sum of $^{40}Ar^*$ and atmospheric ^{40}Ar and the amount of ^{36}Ar isotope of only atmospheric origin, but uncorrected from blank value. They indicate that the BAB formed between 20 and 15Ma and the IAT between 15 and 9Ma.

TABLE IV. – Selected $^{40}K/^{40}Ar$ whole-rock ages of selected BABB (ABN1a, ABN6c and SM16d) and IAT (ABN1j and ABN6a).

TABL. IV. – *Datations radiogéniques (méthode $^{40}K/^{40}Ar$ sur roche totale) de basaltes arrière-arc* (ABN1a, ABN6c *et* SM16d) *et de tholéiites d'arc* (ABN1j *et* ABN6a) *représentatifs de Seram-Ambon.*

	ABN1a BABB	ABN6c BABB	SM16d BABB	ABN6a IAT	ABN1j IAT
$^{40}Ar^*$ (%)	13	12.1	9.6	22.2	14.9
^{40}Ar (e-7 cc/g)	0.84	5.35	0.57	2.27	1.14
^{36}Ar (e-7cc/g)	1.91	1.31	1.83	2.69	2.21
$^{40}K/^{40}Ar$ Age (±) Ma	19.3 ±1.6	15.0 ±1.3	19.7 ±2.0	8.9 ±0.36	15.3 ±1.2

DISCUSSION

The peridotite phase chemistry, and particularly the high Cr# contents of spinels and pyroxenes, illustrate their residual feature. But surprisingly, it is more pronounced in the Pl-lherzolites, and to lesser extent in the Cpx-rich harzburgites, than in the Cpx-free harzburgites. The fact that both spinels and pyroxenes from the Pl-lherzolites and of a few Cpx-rich harzburgites also display unusual high Ti contents indicate that the rocks suffered sub-solidus reequilibration which has led to plagioclase crystallization when the rocks arrived at shallow levels, in the plagioclase field [Kornprobst and Tabit, 1988 ; Li, 1991 ; Cornen *et al.*, 1996 ; Charpentier, 2000]. In agreement with their mineral composition, the Cpx-free harzburgites display low REE concentrations (0.1 to 0.04 times the chondrites for HREE and LREE respectively) and patterns typical of strongly melted rocks. They however display slight LREE enrichments (fig. 4C) as also seen in most of the Cpx-rich harzburgites. These enrichments are commonly interpreted to reflect chromatographic effects resulting from ion exchange reactions between a percolating melt and these peridotites (e.g. Takazawa *et al.* [1992 ; 2000]). However, we cannot exclude a metasomatic process for their origin, particularly for samples KBB17b and Kbb18c (Cpx-rich harzburgites) that show significative LREE enrichment [Wiechert *et al.*, 1996].

Spinels from the Cpx-free harzburgites have very low Cr# contents (Cr#~0.40), which is inconsistent with their low HREE abundances (Lu~0.34 the chondrites) and also very uncommon for abyssal harzburgites [Niu, 1997 ; Niu and Hékinian, 1997]. This likely indicates that the harzburgites result from interaction of their surrounding lherzolites with low-silica activity melts. We believe that the small amount of modal plagioclase present in these Cpx-free harzburgites (fig. 3D) is the result of metasomatism in relation with the metamorphic formation of the plagioclase in the neighbouring Pl-lherzolites, which is also in agreement with the LREE enrichments seen in the harzburgites. If true, this would indicate that the sub-solidus reequilibration event has post-dated the harzurgite formation.

The IAT display low SiO_2 and K_2O concentrations as in basaltic to basalt-andesitic magmas. They have mostly high-Mg contents (MgO>10 wt %) and high Ni and Cr concentrations (up to 200 and 360 ppm in average, respectively) like high-Mg arc-tholeiites. According to Jonhson *et al.* [1980 ; 1990]), such a chemical signature is typical of magmas generated within the mantle wedge during the pristine stage of slab subduction.

As evidenced by their REE patterns, the other volcanic rocks from Seram and Ambon islands are MORB-like. However, their trace element abundances, particularly their LILE enrichments and strong Nb-negative anomalies ($(La/Nb)_N$=3.54 in average), are characteristic of BABB [Saunders and Tarney, 1984 ; Monnier *et al.*, 1995]. Owing to their high Th/Nb ratios (Th/Nb=0.62 in average), it is suggested that they formed along a continental margin crust as already proposed by [Auzende *et al.*, 1990 ; Eissen *et al.*, 1998]. However, some of the BABB (samples ABN1a and ABN1e) display high MgO contents (10-15 wt %), high Ni and Cr concentrations (up to 265 and 500 ppm respectively) and very low SiO_2 contents (<48 wt %) like sub-alkaline magmas. It is proposed that such lavas were emplaced during the first phases of formation of a back-arc basin.

Group 1 gabbros and type 1 websterites display BABB chemical features. Owing to their REE concentrations, they likely crystallized from melts extracted from depleted-peridotites. On the other hand, variations in their REE concentrations are indicative of fractional crystallization processes as occur in cumulates generally sampled in the upper mantle parts of the ophiolitic complexes and linked to the crust formation. In Seram, where they constitute intrusions within the mantle rocks, they may however represent injections contemporaneous with the beginning of the opening of the back-arc basin.

This is also the case of group 2 gabbros and type 2 websterites, although they are slightly different from group 1 gabbros and type 1 websterites. If type 2 websterites likely also originated from a BABB source, as suggested by their trace elements patterns and particularly their negative anomalies of HFSE, group 2 gabbros appear chemically un-

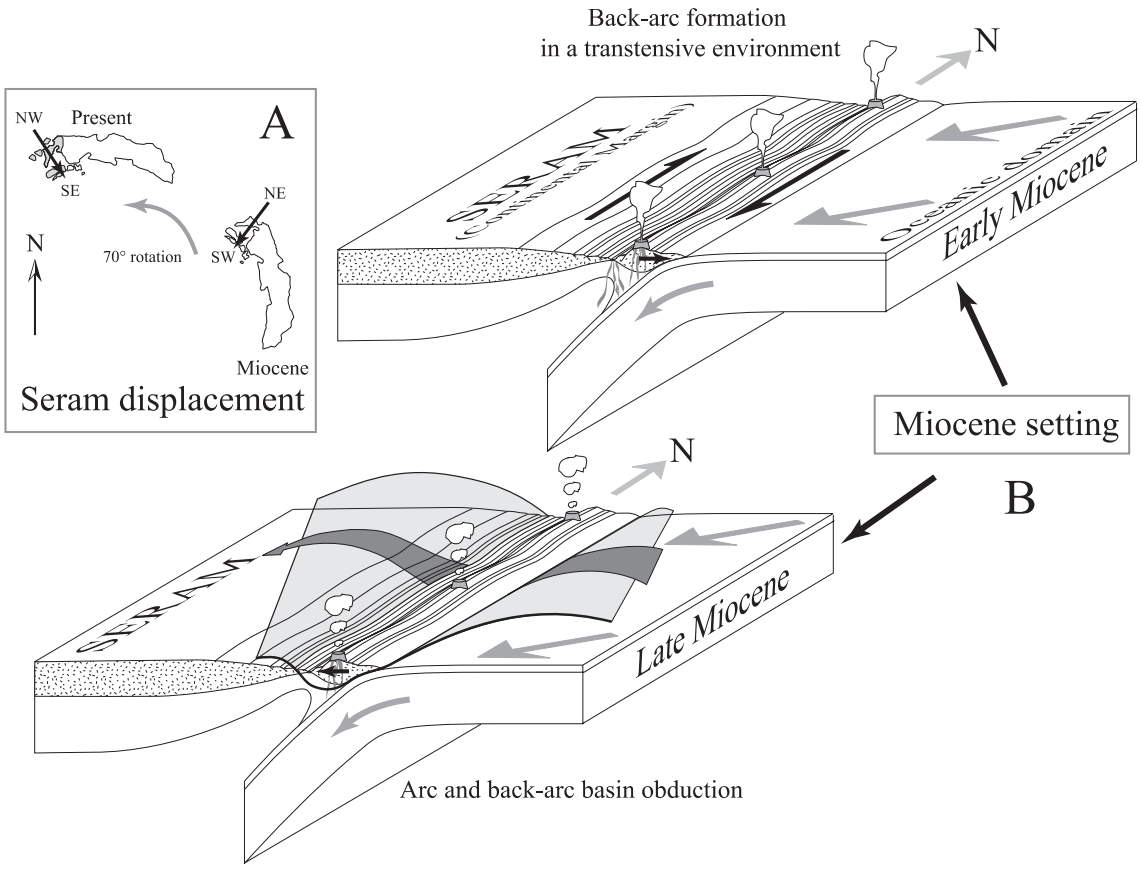

FIG. 7. – Sketch diagrams for the evolution of the Seram-Ambon ophiolites during the Miocene. A) Seram displacement from Miocene to Present assuming the geodynamic reconstruction by Haile [1979 ; 1981] and B) opening of a marginal back-arc basin related to the oblique subduction of an oceanic domain along the Seram continental margin during the early Miocene (shear sense assuming the geodynamic reconstruction by Haile [1979 ; 1981]), and during the late Miocene, SW obduction of parts of the back-arc basin and associated volcanic arc onto the Seram micro-block.
FIG. 7. – *Evolution des ophiolites de Seram-Ambon au cours du Miocène.* A) *déplacement de l'île de Seram depuis le Miocène à l'Actuel, ouverture selon la reconstruction géodynamique de Haile [1979 ; 1981] et* B) *ouverture d'un bassin marginal arrière-arc liée à la subduction oblique d'un domaine océanique situé en bordure de la marge continentale de l'île de Seram au Miocène inférieur, puis obduction vers le SW d'une partie du bassin arrière-arc et de l'arc volcanique associé sur le microbloc de Seram au Miocène supérieur.*

related with previous rocks as they do not bear significant HFSE anomalies. They rather crystallized from a depleted MORB mantle source, which is consistent with the back-arc basins formation where BAB melts can result from the mixing of MORB-like sources and arc-like components (e.g. Taylor and Martinez [2003]).

Also, the type 3 websterites (KL2a and KL2b) appear chemically unrelated with previous rocks because of their marked high LREE-enrichments. This suggests an origin from a calc-alkaline melt at their origin, in agreement with their HFSE-depletion and particularly their low Nb concentrations relative to the neighbouring elements. On the other hand, websterite KL2a is characterized by very low HREE concentrations (Lu=0.6 chondritic values) relative to the Sr and La which are enriched (130 ppm and 3.3 ppm, respectively), so that its Sr/Y ratio is >120 and its La/Yb ratio up to 30. This gives to KL2a websterite an adakitic signature and makes likely that it crystallized from a liquid derived from a garnet-bearing source [Defant and Drummond, 1990] rather than from a superficial hydrated peridotite source [Sajona *et al.*, 1993 ; Sajona *et al.*, 1994]. This hypothesis is also supported by the high Na concentrations of the Cpx (fig. 3E) which indicates crystallization under high pressures (e.g. Cornen *et al.*[1999]).

TECTONIC IMPLICATIONS AND CONCLUSIONS

During the Neogene, eastern Indonesia has recorded numerous deformation episodes linked to translations and rotations of micro-continents, their displacements being more and less linked to the opening of small oceanic basins (e.g. Hinschberger *et al.* [2001]). These geotectonic reorganisations are related to the high convergence rates of both the Australian plate that moves northward at ca. 7 $cm.y^{-1}$ and the Philippine/Caroline plates of the which displacement toward the east occurs at ca. 10 $cm.y^{-1}$ [Minster and Jordan, 1978 ; De Mets *et al.*, 1990]. Although it is currently admitted that the Seram island represents a Paleozoic-Triassic continental fragment of the Australian plate, its evolution during the Cenozoic is still a matter of debate [Katili, 1975 ; Hutchison, 1977 ; Audley-Charles *et al.*, 1979 ; Hamilton, 1979 ; De Smet, 1989 ; Daly *et al.*, 1991 ; Linthout *et al.*, 1997].

Our study of the Seram-Ambon ophiolitic series leads to several geological conclusions that can be summarized as follows :

1) the peridotites represent a piece of weakly depleted mantle that locally suffered interaction with low-silica activity melts which has led to the formation of harzburgites

after lherzolites, prior to their re-equilibration in the plagioclase field during their ascent,

2) their associated high-Mg arc-tholeiites were likely generated within a mantle wedge during the early stage of a slab subduction,

3) these high-Mg arc-tholeiites have strong chemical affinities with their associated BABB, which suggests that the arc and the back-arc basin were almost contemporaneous,

4) the high U and Th concentrations and high Th/Nb ratios (0.62 in average) likely indicate that the BABB generated during rifting of a continental margin crust,

5) except for websterite KL2a which bears adakitic affinities, all other websterites represent melts derived from a BABB source,

6) This is also true for group 1 gabbros whereas group 2 gabbros (ABN1k, ABN1b and ABN1c) likely derived from a N-MORB source.

Our 20 to 15 Ma $^{40}K/^{40}Ar$ ages calculated for the BABB and 15-9 Ma for the IAT show that the basin and arc formed in a very short span of time. It is noteworthy that the arc youngest age is that of the beginning of the Kaibobo ultramafic complex obduction onto Seram at 9.5-7 Ma (Linthout *et al.* [1997]).

Considering the paleogeographic scheme presented by Haile [1979 ; 1981] and Linthout *et al.* [1997] who consider that the Seram island was bordered to its east by an oceanic domain during its northward migration in Miocene times and owing to our geochemical and chronological data, we propose that the Seram-Ambon ophiolites formed during the early Miocene in a small, short-lived (10 Ma), transtensive basin bordered on its western part by a passive continental margin and to its east by an active margin (fig. 7). Its obduction in the early Miocene would have occurred from the NE to the SW, if we consider the 70° rotation that the island underwent during its northward migration [Linthout *et al.*, 1997] and the NW to the SE shear senses we have determined in the field (fig. 2, [Permana, 1998]).

Acknowledgements. – This work was supported by the french MAE through the PICS-Indonésie and INSU-CNRS (Géosciences Marines grants). We thank M. Polvé, B. Reynier, M. Valladon (Toulouse) and L. Lemée (Nantes) for their help in ICP-AES and ICP-MS data acquisition and M. Bohn (IFREMER – Brest) who is in charge of the microprobe. We are grateful for the constructive comments of H. Lapierre and other anonymous reviewers.

References

Audley-Charles M.G., Carter J.D., Barber A.J., Norvick A.J. & Tjokrosapoetro (1979). – Reinterpretation of the geology of Seram : implications for the evolution of Banda Arc and northern Australia. – *Geol. Soc. London*, **136**, 547-568.

Auzende J.-M., Boespflug X., Bougault H., Dosso L., Foucher J.-P., Joron J.-L., Ruellan E. & Sibuet J.-C. (1990). – From intracratonic extension to mature spreading in back-arc basin : examples from the Okinawa, Lau and, North Fidji basins. – *Oceanol. Acta*, **10**, 153-163.

Benoit M., Polvé M. & Ceuleneer G. (1996). – Trace element and isotopic characterization of mafic cumulates in a fossil mantle diapir (Oman ophiolite). – *Chem. Geol.*, **134**, 199-214.

Bodinier J.-L., Vasseur G., Vernières J., Dupuy C. & Fabriès J. (1990). – Mechanisms of mantle metasomatism : geochemical evidence from Lherz orogenic peridotite. – *J. Petrol.*, **31**, 597-628.

Charpentier S. (2000). – La zone de transition continent-océan de la marge continentale passive ouest-ibérique : études pétrologique et géochimique des roches magmatiques et mantelliques. – Thèse de Doctorat d'Université, Blaise Pascal – Clermont II, 327 p.

Cornen G., Beslier M.O. & Girardeau J. (1996). – Petrologic characteristics of the ultramafic rocks from the ocean/continental transition in the Iberia abyssal plain. – *Proc. ODP, Sci. Results*, **149**, 377-395.

Cornen G., Girardeau J. & Monnier C. (1999). – Basalts, underplated gabbros and pyroxenites record the rifting process of the West Iberian margin. – *Mineral. and Petrol.*, **67**, 111-142.

Cotten J., Le Dez A., Bau M., Caroff M., Maury R.C., Dulski P., Fourcade S., Bohn M. & Brousse R. (1995). – Origin of anomalous rare-earth element and yttrium enrichments in subaerially exposed basalts : evidence from French Polynesia. – *Chem. Geol.*, **119**, 115-138.

Daly M.C., Cooper M.A., Wilson I., Smith D.G. & Hooper B.G.D. (1991). – Cenozoic plate tectonics and basin evolution in Indonesia. – *Mar. Petrol. Geol.*, **8**, 2-21.

Daly M.C., Hooper B.G.D. & Smith D.G. (1987). – Tertiary plate tectonics and basin evolution in Indonesia. – *Proc. Indon. Petro. Asso.*, **1**, 399-428.

De Mets C., Gordon R.G., Argus D.F. & Stein S. (1990). – Current plate motions. – *Geophys. J. Int.*, **101**, 425-478.

De Smet M., Sumosuastro P.A., Siregar L.J., Van MARLE L., J., Troelstra & Fortuin A.R. (1989). – Cenozoic geohistory of Seram, Indonesia. – *Geol. Mijnb.*, **68**, 221-235.

De Smet M.E.M. (1989). – A geometrically consistent plate tectonic model for eastern Indonesia. *In* : J.E. Van Hinte, T.C.E. Van Weering & A.R. Fortuin, Eds., Proceedings for Snellius II Symposium. Theme ; Geology and geophysics of Banda arc and adjascent areas, Part I. – *Neth. J. Sea Res.*, **24**, 173-183.

Defant M.J. & Drummond M.S. (1990). – Derivation of some modern arc magmas by melting of young subducted lithosphere. – *Nature*, **347**, 662-665.

Eissen J.-P., Crawford A.J., Cotten J., Meffre S., Bellon H. & Delaune M. (1998). – Geochemistry and tectonic significance of basalts in the Poya Terrane, New Caledonia. – *Tectonophysics*, **284**, 203-219.

Haile N.S. (1979). – Paleomagnetic evidence for the rotation of Seram, Indonesia. *In* : S. Uyeda, R.W. Murphy & K. Kobayashi, Eds., Geodynamic of the western Pacific. – *Advance in Earth and Planet. Scie.*, **6**, 191-198.

Haile N.S. (1981). – Paleomagnetic evidence and the geotectonic history and paleogeography of eastern Indonesia. *In* : A.J. Barder & S. Wiryusujono, Eds., The geology and tectonics of eastern Indonesia. – *Indon. Geol. Res. Dev. Centre, Spe. Publ.*, **2**, 81-87.

Hamilton W.B. (1979) – Tectonics of the Indonesia region. – *U.S. Geol; Surv. Prof. Paper* 1078, Denver, 345 p.

Hinschberger F., Malod J.-A., Dyment J., Honthaas C., Réhault J.-P. & Burrhanuddin (2001). – Magnetic lineations constraints for a back-arc opening to the late Neogene south Banda basin (eastern Indonesia). – *Tectonophysics*, **333**, 47-59.

HUTCHISON C.S. (1977). – Banda Sea volcanic arc : some comments on the Rb, Sr and cordierite contents. – *Geol. Soc. Malasya Newslett.*, **3**, 27-35.

JOHNSON K.M., DICK H.J.B. & SHIMIZU N. (1990). – Melting in the oceanic upper mantle : an ion microprobe study of diopsides in abyssal peridotites. – *J. Geophys. Res.*, **95**, 2661-2678.

JOHNSON R.W. & JACQUES A.L. (1980). – Continent-arc collision and reversal of arc polarity : new interpretations from a critical area. – *Tectonophysics*, **63**, 111-124.

KATILI J.A. (1975). – Volcanism and plate tectonics in the Indonesian island arcs. – *Tectonophysics*, **45**, 165-188.

KELEMEN P.B., JOHNSON K.T.M., KINZLER R. & IRVING A.J. (1990). – High field strength element depletions in arc basalts due to mantle : production of harzburgites by mantle-magma interaction. – *Nature*, **358**, 635-640.

KORNPROBST J. & TABIT A. (1988). – Plagioclase-bearing ultramafic tectonites from the Galicia margin (leg 103, site 637) : comparison of their origin and evolution with low-pressure ultramafic bodies in western Europe. *In* : G. BOILLOT & E.L. WINTERER, Eds., Proc. ODP, Sci. Results. – *College Station, TX (Ocean Drilling Program)*, **103**, 253-263.

LI J.P. (1991). – Evolution chimique des phases solides dans la fusion partielle et la rééquilibration de subsolidus des peridotites naturelles : étude expérimentale et applications. – Thèse de Doctorat d'Université Clermont-Ferrand, Université Blaise Pascal, 262 p.

LINTHOUT K. & HELMERS H. (1994). – Pliocene obducted, rotation and migrated ultramafic rocks and obducted-induced anatectic granite, SW Seram and Ambon, eastern Indonesia. – *J. SE Asian Earth Sci.*, **9**, 95-109.

LINTHOUT K., HELMERS H. & SOPAHELUWAKAN J. (1997). – Late Miocene obduction and microplate migration around the southern Banda Sea and the closure of the Indonesia seaway. – *Tectonophysics*, **281**, 17-30.

LINTHOUT K., HELMERS H., SOPAHELUWAKAN J. & SURYA NILA E. (1989). – Metamorphic complexes in Buru and Seram, northern Banda Sea arc. – *Neth. J. Sea Res.*, **24**, 345-365.

LINTHOUT K., HELMERS H., WIJBRANS J.R., DIEDERIK J. & VESS V. (1996). – $^{40}Ar/^{39}Ar$ constraints on obduction of Seram ultramafic complex : consequences for the evolution of the southern Banda Sea. *In* : R. HALL & D. BLUNDELL, Eds., Tectonic evolution of Southeast Asia. – *Geol. Soc. London Spec. Publ.*, 455-464.

MAHOOD G.A. & DRAKE R.E. (1982). – K-Ar dating young rhyolitic rocks : a case study of the Sierra La Primavera, Jalisco, Mexico. – *Geol. Soc. Amer. Bull.*, **93**, 1232-1241.

MAURY R.C., DEFANT M.J. & JORON J.-L. (1992). – Metasomatism of the sub-arc mantle inferred from trace elements in Philippines xenoliths. – *Nature*, **360**, 661-663.

MILSON J. (1977). – Preliminary gravity map of Seram, eastern Indonesia. – *Geology*, **5**, 641-643.

MINSTER J.B. & JORDAN T.H. (1978). – Present-day plate motions. – *J. Geophys. Res.*, **83**, 5331-5354.

MONNIER C., GIRARDEAU J., MAURY R.C. & COTTEN J. (1995). – Back-arc basin origin for the East Sulawesi ophiolite (eastern Indonesia). – *Geology*, **23**, 851-854.

NIU Y. (1997). – Mantle melting and melt extraction processes beneath ocean ridges : evidence from abyssal peridotites. – *J. Petrol.*, **38**, 1047-1074.

NIU Y. & HÉKINIAN R. (1997). – Basaltic liquids and harzburgitic residues in the Garrett Transform : a case study at fast-spreading ridges. – *Earth Planet. Sci. Lett.*, **146**, 243-258.

ODIN G.S. (1994). – Geological time scale. – *C. R. Acad. Sci.,* Paris, II, **318**, 57-67.

PARKINSON I.J., PEARCE J.A., THIRLWALL M.F., JONHSON K.T.M. & INGRAM G. (1992). – Trace element geochemistry of peridotites from Izu-Bonin-Mariana forearc, Leg 125. – *Proc. ODP, Sci. Results*, **125**, 487-506.

PERMANA H. (1998). – Dynamique de mise en place des ophiolites d'Irian Jaya (Indonésie). – Thèse de Doctorat d'Université Nantes, Nantes, 313 p.

SAJONA F.G., BELLON H., MAURY R.C., PUBELLIER M., COTTEN J. & RANGIN C. (1994). – Magmatic response to abrupt changes in tectonic settings : Pliocene-Quaternary calc-alkaline and Nb-enriched lavas from Mindanao (Philippine). – *Tectonophysics*, **237**, 47-72.

SAJONA G.S., MAURY R.C., BELLON H., COTTEN J., DEFANT M. & PUBELLIER M. (1993). – Initiation of subduction and the generation of slab melts in western and eastern Mindanao, Philippines. – *Geology*, **21**, 1007-1010.

SAUNDERS A.D. & TARNEY J. (1984). – Geochemical characteristics of basalt volcanism within back-arc basins. *In* : B.P. KOKELAAR & M.F. HOWELL, Eds., Marginal basin geology : volcanic and associated sedimentary and tectonic processes in modern and ancient marginal basins. – *Geol. Soc. London Spec. Publ.*, **16**, 57-76.

STEIGER R.H. & JÄGER E. (1977). – Subcommission on geochronology : convention on use of decay constants in geo– and cosmochronology. – *Earth Planet. Sci. Lett.*, **26**, 359-362.

SUN S.S. & MCDONOUGH W.F. (1989). – Chemical and isotopic systematics of oceanic basalts : implications for mantle composition and processes. *In* : A.D. SAUNDERS & J.M. NORRY, Eds., Magmatism in the ocean basins. – *Geol. Soc. London Spec. Publ.*, **42**, 313-345.

TAKAZAWA E., FREY A.F., SHIMIZU N., OBATA M. & BODINIER J.L. (1992). – Geochemical evidence for melt migration and reaction in the upper mantle. – *Nature*, **359**, 55-58.

TAKAZAWA E., FREY F.A., SHIMIZU N. & OBATA M. (2000). – Whole rock composition variations in an upper mantle peridotites (Horoman, Hokkaido, Japan) : are they consistent with a partial melting process ? – *Geochim. Cosmochim. Acta*, **64**, 695-716.

TAYLOR B. & MARTÍNEZ F. (2003). – Back-arc basin basalt systematics. – *Earth Planet. Sci. Lett.*, **210**, 481-497.

TJOKROSAPOETRO S. & BUDHITRISNA T. (1982). – Geology and tectonics of the northern Banda arc. – *Indon. Geol. Res. Dev. Centre, Spec. Publ*, **6**, 1-17.

WIECHERT U., IONOV D.A. & WEDEPOHL K.H. (1996). – Spinel peridotite xenoliths from the Atsagin-Dush volcano, Dariganga lava plateau, Mongolia : a record of partial melting and cryptic metasomatism in the upper mantle. – *Contrib. Mineral. Petrol.*, **126**, 345-364.